Revision 1

Word Count: 6195

Systematic study of high field strength elements during liquid immiscibility between carbonatitic melt and silicate melt

Wanzhu Zhang[1], Shuo Xue[2,3*], Ming-Xing Ling[1*], Xing Ding[4]

[1]State Key Laboratory of Nuclear Resources and Environment, East China University of Technology, Nanchang 330013, China

[2]CAS Key Laboratory of Mineralogy and Metallogeny, Guangzhou Institute of Geochemistry, Chinese Academy of Sciences, Guangzhou 510640, China

[3]CAS Center for Excellence in Deep Earth Science, Guangzhou 510640, China

[4]State Key Laboratory of Isotope Geochemistry, Guangzhou Institute of Geochemistry, Chinese Academy of Sciences, Guangzhou 510640, China

ABSTRACT

Natural carbonatites exhibit a wide range of high field strength elements (HFSEs) and the highest Nb/Ta and Zr/Hf ratios of among various rock types. However, primitive carbonatitic melts derived from carbonated peridotite do not do not display significant fractionation of Nb-Ta and Zr-Hf. To investigate this further, we conducted liquid immiscibility experiments to comprehend the differentiation of these HFSEs. Our

* Corresponding author. E-mail address: xueshuo@gig.ac.cn
* Corresponding author. E-mail address: mxling@ecut.edu.cn

experiments revealed substantial changes in partition coefficients for Nb, Ta, Zr, and Hf between carbonatite and silicate melts. We identified a positive correlation between partition coefficients of these elements and Si, indicating that Si determines the differentiation of Nb-Ta and Zr-Hf during liquid immiscibility. The partition coefficients of Si increase as temperature decreases and pressure increases, resulting in higher HFSE concentrations during the early stages of liquid immiscibility. Liquid immiscibility is crucial in differentiating HFSEs in carbonatitic melts, explaining the association between super large carbonatite-related Nb deposits and Si-undersaturated silicate rocks.

Keywords: High field strength elements (HFSE); Liquid immiscibility; Carbonatitic and silicate melt; Piston-cylinder experiments

INTRODUCTION

The high field strength elements (HFSEs, including Nb, Ta, Zr and Hf) serve as a valuable tool to study the geochemical processes in the upper mantle and continental crust (Pfänder et al., 2007; Tang et al., 2019). The unique properties of HFSE (e.g., high melting points, good corrosion resistance and biocompatibility) make them highly valuable from aerospace and defense to consumer electronics and medical devices (Mackay and Simandl, 2014). The demand for HFSEs is expected to continue to grow as technology advances and new applications are developed. However, the availability of these elements may be limited due to their relative scarcity in the Earth's crust, and

discovering and exploring new deposits of HFSEs will require significant investment from the geological community.

The majority of the world's resources of HFSEs are closely related with carbonatite and related alkaline silicate rocks (Mitchell, 2005; Mitchell, 2015). However, only 50 out of 609 (~10%) carbonatites have the potential for enriching REE and HFSE to economic ore grade (Anenburg et al., 2021; Humphreys-Williams and Zahirovic, 2021; Woolley and Kjarsgaard, 2008). Therefore, the formation of carbonatite-related deposits requires more stringent conditions. In addition, Zr-Hf and Nb-Ta are considered as elemental twins and exhibit very similar geochemical behaviors throughout various geological processes. Nevertheless, natural carbonatites from different geological settings often exhibit a significant variability in their HFSEs concentrations, Zr/Hf and Nb/Ta ratios (see Figure S1) (Bizimis et al., 2003; Chakhmouradian, 2006; Hoernle et al., 2002; Rudnick et al., 1993), implying that Zr and Hf, as well as Nb and Ta, were fractionated from each other during the formation and evolution of carbonatites.

The formation of carbonatite rocks typically begins with partial melting of carbonated mantle peridotite or eclogite, resulting in the formation of initial carbonatitic melts or CO_2-rich alkali silicate melts (Dasgupta and Hirschmann, 2006; Dasgupta et al., 2013; Rudnick et al., 1993; Wallace and Green, 1988). These initial melts undergo either liquid immiscibility or fractional crystallization, which leads to the evolution of natural carbonatites (Brooker and Kjarsgaard, 2011; Kjarsgaard and Hamilton, 1989; Lee and

Wyllie, 1994; Martin et al., 2013; Mitchell, 2005; Nabyl et al., 2020; Tappe et al., 2017; Veksler et al., 1998; Yaxley et al., 2022). All these processes have the potential to determine the concentration and differentiation of HFSEs. To fully understand the contribution of these processes, further studies are necessary to develop a comprehensive understanding of the partition coefficients between minerals and carbonatitic melts, as well as the partition coefficients between silicate melts and carbonatitic melts. Previous experimental studies have investigated the partitioning of HFSEs between carbonatitic melts and the primary minerals found in the mantle, such as clinopyroxene (cpx), garnet, orthopyroxene (opx), and olivine (Adam and Green, 2001; Blundy and Dalton, 2000; Brenan and Watson, 1991; Dasgupta et al., 2009; Green et al., 1992; Klemme et al., 1995; Sweeney et al., 1995). However, there is currently a lack of sufficient experimental data on HFSEs partitioning between carbonatitic melts and silicate melts.

Previous studies shown that the partition coefficients of HFSEs between carbonatitic melts and silicate melts can vary by 1–3 orders of magnitude under different temperature, pressure, oxygen fugacity, and compositions (Martin et al., 2013; Martin et al., 2012; Nabyl et al., 2021; Nabyl et al., 2020; Veksler et al., 1998; Veksler et al., 2012). This limited dataset has resulted in significant uncertainties in estimating the impact of liquid immiscibility on HFSEs. These uncertainties are necessary to evaluate the geochemical consequences of carbonatitic melt generation in the upper mantle and crust. Additionally, the role of halogens such as fluorine and sulfate on HFSEs behavior during immiscibility

will be further investigated by incorporating various proportions of fluorine and sulfate in our experiments. This study aims to investigate the partition coefficients of Nb-Ta-Zr-Hf between carbonatitic melt and silicate melts at 1000–1300 °C and 0.5–2.2 GPa and to discuss the causes and significance of the observed variations.

PISTON-CYLINDER EXPERIMENTS

Piston-cylinder experiments were conducted at the Guangzhou Institute of Geochemistry, Chinese Academy of Sciences to study partitioning behavior. The starting material used in these experiments was a mixture composition (#RB100) obtained from Brooker and Kjarsgaard (2011), consisting of reagent-grade SiO_2, Al_2O_3, $CaCO_3$, and Na_2CO_3 (as detailed in Table 1). To introduce HFSEs and other trace elements, a small fraction (~100 ppm) of trace element oxide powder was added to the mixture. Additionally, different quantities of MgF_2 and $CaSO_4$ were added to introduce fluorine and sulfate, respectively. The mixture was mixed in an agate mortar for 4–5 hours to ensure the homogenization of the starting powders. All synthetic powders were stored in a dry oven at 120 °C to maintain their integrity and dryness.

To initiate the experiments, approximately 20 mg of the starting material was loaded into 2 mm diameter Pt capsules and subjected to pressures ranging from 0.5–2.2 GPa and temperatures ranging from 1000–1200°C. The Pt capsules were placed in an MgO tube and sealed at both ends with MgO plugs, which were loaded into a ½-inch piston-cylinder

assembly made up of graphite, pyrex, and NaCl cylinders. Temperature was monitored using a S-type thermocouple ($Pt_{94}Rh_6$-$Pt_{70}Rh_{30}$) positioned on bottom of the sample. The experimental samples were slowly pressurized to the target pressure. Subsequently, the assembly was heated to a temperature higher than the desired temperature (1300 °C) for 2 hours before slowly cooling to the target temperature. The experiments were completed with an isobaric quench by switching off the heating source at constant pressure. The uncertainties in temperature and pressure were ±10 °C and ±0.1 GPa, respectively. The experimental conditions and run products are summarized in Table 2.

RESULTS

Experimental products and composition of immiscible melts

The experiments resulted in the production of immiscible liquid phases, which consisted of carbonatitic liquids and quenched alkaline silicate melts (as shown in Figure 1). Backscattered Electron (BSE) images reveal spherical silicate liquids enclosed by rapidly cooled carbonatitic melt. The silicate melt solidified into homogeneous spherical glasses, while the carbonatitic melt formed dendritic crystals of carbonates and silicates, which are typical textures of unquenchable carbonatitic liquids (Brooker and Kjarsgaard, 2011; Martin et al., 2013). This demonstrates that the immiscible liquids reached a state of equilibrium at the experimental pressure-temperature conditions. Major and trace element compositions of the quenched carbonatitic melt and silicate melt were measured

using electron probe microanalyzer (EPMA) and LA–ICP–MS with large beam sizes (Table S1 and S2). Detailed experimental analysis methods are provided in the supplementary materials (Text S1 and S2). The chemical composition of each liquid phase was homogeneous, further confirming the attainment of equilibrium. The focus of this research is to discuss the distribution characteristics of HFSE in the experimental products.

The concentrations of HFSE in the carbonatitic and silicate melt phases were measured using LA–ICP–MS (Table S1 and S2). The standard deviations on the compositions of each phase attest to the homogeneity of the run products and attainment of equilibrium. The HFSE concentrations of the carbonatitic melt ranged from 51.4±0.71 to 92.5±4.83 ppm for Nb, and from 31.7±6.79 to 113±2.28 ppm for Ta, from 15.8±1.58 to 86.6±3.61 ppm for Zr, and from 8.69±0.60 to 81.1±2.05 ppm for Hf. On the other hand, the silicate melt HFSE concentrations were higher than coupled carbonatitic melt, varying from 75.3±1.69 to 190±4.14 ppm for Nb, from 180±1.66 to 330±4.31 ppm for Ta, from 153±8.46 to 265±11.1 ppm for Zr and from 185±3.76 to 300±2.01 ppm for Hf. Our findings showed a positive correlation between the SiO_2 contents in both silicate and carbonatitic melts and the concentration of Nb, Ta, Zr and Hf, indicating that these elements mainly replace the position of Si in the carbonatite-silicate melts (Figure S2 and S3).

Trace elements partitioning between carbonatitic and silicate melts

This is the peer-reviewed, final accepted version for American Mineralogist, published by the Mineralogical Society of America.
The published version is subject to change. Cite as Authors (Year) Title. American Mineralogist, in press.
DOI: https://doi.org/10.2138/am-2023-9093. http://www.minsocam.org/

Trace element partitioning is defined using the Nernst partition coefficient D which corresponds to the mass concentration ratio in ppm of the element i in the carbonatitic melt (CM) and the silicate liquid (SL; $D_i^{CM/SL} = C_i^{CM}/C_i^{SL}$). HFSE partition coefficients between carbonatitic melts and silicate liquids are presented in Table 3. For most of the experimental conditions, silicate liquids are richer in HFSE than the coexisting carbonatitic melts (Table 3), but the partition coefficients vary greatly, from 0.44±0.07 to 0.83±0.05 for Nb, from 0.10±0.01 to 0.61±0.02 for Ta, from 0.06±0.01 to 0.45±0.02 for Zr, and from 0.03±0.00 to 0.43±0.01 for Hf. No clear effect of sulfate and fluorine on HFSE partitioning is identified in the non-doped system and the SO_4^{2-} and F-rich systems (Figure S4). The highest HFSE partition coefficients correspond to the less evolved carbonatite and silicate melts, in other words to the most differentiated carbonatite and silicate melts.

Some of the samples appear to have higher concentrations of F^- and SO_4^{2-} compared to others. However, no clear correlation between $D_{HFSE}^{CM/SL}$ and the concentration of F^- and SO_4^{2-} in the carbonatitic melt has been observed so far, as can be seen in Supplementary Figure S4. This lack of correlation is consistent with previous findings (Nabyl et al., 2021). HFSEs tend to concentrate in silicate melts ($D_{HFSE}^{CM/SL} < 1$), which can coexist with both F^-/SO_4^{2-}-rich and F^-/SO_4^{2-}-poor experimental runs. Additionally, Table 3 indicates that there is no relationship between HFSEs and either F or SO_4^{2-} partitioning. These observations suggest that there is no significant direct effect of fluorine and sulfate

concentrations on the HFSEs partitioning between carbonatite and silicate melts.

DISCUSSION

Parameters controlling the partitioning behavior of high field strength elements

The partition coefficients of high field strength elements between carbonatitic melt and silicate melt ($D_{HFSE}^{CM/SL}$) in this study have been compared to previous investigations (Figure S5). Both our experiments and previous partitioning experiments have demonstrated that immiscibility processes between silicate and carbonatitic melts can result in the depletion of HFSEs in carbonatitic melts, depending on varying temperature, pressure, and compositional conditions (Martin et al., 2013; Nabyl et al., 2020; Veksler et al., 1998; Veksler et al., 2012). The newly obtained $D_{HFSE}^{CM/SL}$ in this study are consistent with recent partitioning experiments (Martin et al., 2013; Nabyl et al., 2021; Nabyl et al., 2020), but significantly higher than the experimental results of Veksler and coworkers (Veksler et al., 1998; Veksler et al., 2012). Noteworthy, our experiments show that HFSE partition coefficients essentially vary in response to changes in the melt composition, especially the SiO_2 content (Figure 2). This phenomenon can be attributed to the similar geochemical behavior of HFSE with silicon, as HFSE tend to replace Si in the structural positions of the melt. Besides, the increase of $D_{Si}^{CM/SL}$ also promote the differentiation between Nb-Ta and Zr-Hf, as shown in Figure 2.

If the oxidation state of HFSE (M) in silicate melt is 4+, the carbonatitic

This is the peer-reviewed, final accepted version for American Mineralogist, published by the Mineralogical Society of America.
The published version is subject to change. Cite as Authors (Year) Title. American Mineralogist, in press.
DOI: https://doi.org/10.2138/am-2023-9093. http://www.minsocam.org/

melt/silicate melt partitioning of HFSE (M) can be described as:

$$MO_2(CM) + SiO_2\ (SL) = MO_2(SL) + SiO_2(CM) \quad \text{Eq. (1)}$$

The equilibrium constant (k) of Eq. (1) can be written as:

$$k_{Eq.(1)} = \frac{\alpha_{MO_2}^{SL} \cdot \alpha_{SiO_2}^{CM}}{\alpha_{MO_2}^{CM} \cdot \alpha_{SiO_2}^{SL}} \quad \text{Eq. (2)}$$

$$k_{Eq.(1)} = \frac{x_{MO_2}^{SL} \cdot \gamma_{MO_2}^{SL} \cdot x_{SiO_2}^{CM} \cdot \gamma_{SiO_2}^{CM}}{x_{MO_2}^{CM} \cdot \gamma_{MO_2}^{CM} \cdot x_{SiO_2}^{SL} \cdot \gamma_{SiO_2}^{SL}} \quad \text{Eq. (3)}$$

where α, x, and γ denote activity, mole fraction, and activity coefficient, respectively. Eq. (4) can be further written as:

$$logK_{Eq.(1)} = \log\left(\frac{x_{SiO_2}^{CM}}{x_{SiO_2}^{SL}}\right) - \log\left(\frac{x_{MO_2}^{CM}}{x_{MO_2}^{SL}}\right) + \log\left(\frac{\gamma_{MO_2}^{SL} \cdot \gamma_{SiO_2}^{CM}}{\gamma_{MO_2}^{CM} \cdot \gamma_{SiO_2}^{SL}}\right) \quad \text{Eq. (4)}$$

$logK_{Eq.(1)}$ can also be thermodynamically expressed as:

$$logK_{Eq.(1)} = -\Delta G^0/RT = -(\Delta H_r^0 - T\Delta S_r^0 + \int \Delta V dP)/RT \quad \text{Eq. (5)}$$

where R is gas constant, ΔG^0 is Gibbs free energy, ΔH_r^0 is enthalpy change, ΔS_r^0 is entropy change, and ΔV is volume change for the reaction of Eq. (1). Assuming that $\gamma_{MO_2}^{SL}$, $\gamma_{SiO_2}^{CM}$, $\gamma_{MO_2}^{CM}$, and $\gamma_{SiO_2}^{SL}$ do not vary greatly with the variation of melt composition and temperature, the following equation can be obtained from Eqs. (4) and (5):

$$logD_M^{CM/SL} = \frac{a}{T} + b \cdot \frac{P}{T} + c + \mathrm{d} \cdot \log\left(D_{Si}^{CM/SL}\right) \quad \text{Eq. (6)}$$

Therefore, the $D_{HFSE}^{CM/SL}$ is a function of T, P and melt compositions (especially SiO_2). We have derived an empirical model (Eq. 6) in which T, P and $D_{Si}^{CM/SL}$ are the only required input parameters.

The findings of this study highlight the importance of understanding the partitioning behavior of Si during immiscibility, considering its similarity in geochemical behavior

with HFSEs. Our experiments suggest that temperature and pressure both play significant roles in the partitioning of Si, with decreasing temperature and increasing pressure both resulting in increased $D_{Si}^{CM/SL}$ (as seen in Figure S6). These findings are in line with previous studies (Brooker and Kjarsgaard, 2011; Freestone and Hamilton, 1980; Hamilton et al., 1989). Consequently, we propose that temperature and pressure primarily impact the partitioning of major elements (SiO_2), which in turn affects the partitioning of HFSEs.

Effects of liquid immiscibility on high field strength elements

Under mantle and crustal pressure, primitive carbonatitic melts can undergo a separation into carbonatite and silicate melts through liquid immiscibility (Berndt and Klemme, 2022; Hamilton and Kjarsgaard, 1993; Lee and Wyllie, 1997; Weidendorfer and Asimow, 2022). This process plays an important role in the petrogenesis and mineralization processes of carbonatites. Liquid immiscibility has been observed to decrease the SiO_2, Al_2O_3, MgO contents, while increase CaO content in the resulting evolved carbonatitic melt (Brooker and Kjarsgaard, 2011). In addition, liquid immiscibility can lead to the enrichment of rare earth elements (REE) in Ca-rich carbonatitic melts compared to conjugate silicate melts, which is favorable for the formation of rare earth deposits (Martin et al., 2013; Nabyl et al., 2020). However, the effect of liquid immiscibility on the modification and fractionation of HFSEs during this process remains unclear.

This is the peer-reviewed, final accepted version for American Mineralogist, published by the Mineralogical Society of America.
The published version is subject to change. Cite as Authors (Year) Title. American Mineralogist, in press.
DOI: https://doi.org/10.2138/am-2023-9093. http://www.minsocam.org/

In order to quantitatively assess the impact of liquid immiscibility on HFSEs, we employed our newly obtained $D_{HFSE}^{CM/SL}$ values (as depicted in Figure 3) to model various carbonatite immiscibility proportions from primitive CO_2-rich silicate melts. We are attempting to simulate the separation of the initial CO_2-rich alkaline silicate melt into silicate melt and carbonatitic melt under the temperature and pressure conditions of the crust. In our modeling, we assumed that the mass of the initial CO_2-rich alkaline silicate melt (IM) is M_0, and the concentration of element i is C_0. After the liquid immiscibility occurs, the mass ratio of the differential carbonatitic melt (CM) and the initial melt is F. The concentration of element i in the carbonatitic melt and silicate melt are C_{CM} and C_{SL}, respectively. D represents the partition coefficients of element i between carbonatitic melt and silicate melt and D equals the C_{CM} divided by the C_{SL}.

Based on the mass balance calculation, we described the liquid immiscibility using equation (7):

$$C_0 \times M_0 = C_{CM} \times F \times M_0 + C_{SL} \times (1 - F) \times M_0 \quad \text{Eq. (7)}$$

Based on the definition of partition coefficient (D):

$$C_{SL} = C_{CM}/D \quad \text{Eq. (8)}$$

Substituting Eq. (8) into Eq. (7) yields:

$$C_{CM} = C_0 \times ((1 - F)/D + F)^{-1} \quad \text{Eq. (9)}$$

From Eq. (9), it can be seen that the concentration of element i in the carbonatitic melt mainly depends on the choice of partition coefficient (D) and the proportion of

carbonatitic melt after the liquid immiscibility (F). According to our previous discussion, it has been found that the partition coefficients of HFSEs are mainly determined by the partition behavior of the major element Si. The different $D_{Si}^{CM/SL}$ represent the separation of carbonatitic and silicate melts at different stages. As carbonated silicate magma evolves to a later stage and liquid immiscibility occurs, it will cause the $D_{Si}^{CM/SL}$ to decrease. To assess the distribution of HFSEs, we categorized it into two scenarios, one with high $D_{Si}^{CM/SL}$ and another with low $D_{Si}^{CM/SL}$. We determined the distribution coefficient of HFSEs based on high $D_{Si}^{CM/SL}$ and low $D_{Si}^{CM/SL}$. For high $D_{Si}^{CM/SL}$, we defined the $D_{Nb}^{CM/SL}$ equals 0.73, the $D_{Ta}^{CM/SL}$ equals 0.61, the $D_{Hf}^{CM/SL}$ equals 0.43, and the $D_{Zr}^{CM/SL}$ equals 0.45. For low $D_{Si}^{CM/SL}$, we choose the $D_{Nb}^{CM/SL}$, $D_{Ta}^{CM/SL}$, $D_{Hf}^{CM/SL}$, $D_{Zr}^{CM/SL}$ as 0.31, 0.08, 0.05, 0.07, respectively. The initial HFSE contents in the primitive CO_2-rich carbonatitic melt were based on melts derived from carbonated peridotite near the solidus. Please refer to Table 4 for a detailed description of the modeling procedure.

Simulation results indicate that liquid immiscibility can cause varying degrees of depletion of HFSEs in fractionated carbonatitic melts. Lower Si partition coefficients will lead to the depletion of HFSEs in carbonatitic melts up to an order of magnitude. Although liquid immiscibility can cause varying degrees of depletion of HFSEs, it still cannot fully explain the six to seven orders of magnitude variation range of these elements in natural carbonatites. In addition, our modelling results show that the Nb/Ta (59–89) and Zr/Hf (27–54) ratios in the carbonatitic melts increase with decreasing

proportion of carbonatitic melt due to liquid fractionation. However, this change is also less than one magnitude and cannot fully explain the large variation of Nb/Ta and Zr/Hf ratios observed in natural carbonatites.

Implication for HFSE mineralization in carbonatite

High field strength element deposits are commonly associated with carbonatite and alkaline rocks, with well-known deposits including Araxá in Brazil, Mount Weld in Australia, Kipawa in Canada, Tomtor and Kovdor in Russia, Bayan Obo and Huayangchuan in China (Aral and Bruckard, 2008; de Oliveira Cordeiro et al., 2011; Fowler et al., 2002; Ivanyuk et al., 2016; Lazareva et al., 2015; Ling et al., 2013; Xue et al., 2020; Yang et al., 2023). Araxá is particularly noteworthy, as it is one of the largest carbonatite-type Nb-Ta deposit in the world, with mineralization primarily hosted in pyrochlore and columbite-tantalite minerals (Mitchell, 2015). However, despite the close spatial relationship between carbonatite and HFSE deposits, only less than 5% of carbonatites are mineralized, indicating that strict conditions are necessary for HFSE mineralization in carbonatite.

Our hypothesis is that a higher concentration of HFSE in carbonatitic melts, which have undergone liquid immiscibility, may be conducive to later mineralization. Here, we assume two scenarios: one is that immiscibility occurs at relatively shallow depths and high temperatures, and the other is that it occurs at deeper depths and lower temperatures in the crust (Figure 4). Under the first scenario, the differentiated carbonatitic melt

contains a higher SiO_2 content compared to the second scenario, where the SiO_2 content is lower in carbonatitic melt. This leads to a higher partition coefficient of Si and enrichment of HFSE in the carbonatitic melt, thereby creating favorable conditions for mineralization. Our research demonstrates that Si-rich carbonatites that are in equilibrium with Si-poor alkaline silicate magmas (e.g., ijolite and nephelinite) are the most enriched in HFSEs and are therefore the most promising targets for mineralization. This may explain the association between the world's largest Nb (Araxá deposit) ore deposit and melilitite and nephelinite, which have low SiO_2 and high CaO content compared to other types of alkaline complexes (Mitchell, 2005; Mitchell, 2015).

The formation of giant HFSE deposits can be facilitated by liquid immiscibility, but the pre-enrichment of HFSE in the mantle source also plays a crucial role (Xue et al., 2020). Additionally, the process of crystallization differentiation and post-magmatic fluid exsolution can enhance HFSE enrichment and redistribution. In this study, we have collected data on the major and trace element contents of both Nb mineralized and non-mineralized carbonatite-silicate complex. The compiled data are presented in Supplementary Table S3. The mineralized carbonatite-silicate complex data primarily originate from Miaoya (China), Bayan Obo (China), and Araxá (Brazil). The non-mineralized carbonatite-silicate complex data is sourced from Weishan (China), Mianning-Dechang Belt (China), Mountain Pass (America) (Castor, 2008; Hou et al., 2015; Hou et al., 2006; Liu et al., 2019; Palmieri et al., 2022; Poletti et al., 2016; Su et al.,

2019; Verplanck et al., 2016; Wang et al., 2019; Wang et al., 2001; Xu et al., 2003; Yang et al., 2023; Zhang et al., 2019). Our data compilation revealed that both carbonatites and silicate rocks in mining districts exhibit higher Nb contents and relatively lower SiO_2 contents (Figure S7). This emphasizes the crucial role of initial magma Nb content in determining the potential for later mineralization. Furthermore, the liquid immiscibility leading to the formation of silicate melts with lower SiO_2 content appears to favor Nb partitioning into carbonatitic melts. This is consistent with the conclusions drawn from our current experiments. Additionally, natural carbonatite and syenite rocks have higher Nb/Ta and Zr/Hf ratios (Figure S7), which may be due to differences in the Nb/Ta and Zr/Hf ratios in the mantle, as well as later crystallization differentiation. For example, initial silicate melts formed from mantle source with high Nb/Ta ratios would result in higher Nb/Ta ratios. Moreover, Ta is relatively more compatible with Nb, and Hf is more compatible with Zr. The separation and crystallization of certain minerals such as perovskite, zircon, and amphibole can lead to the depletion of Ta, Zr, and Hf (Adam and Green, 2001; Dasgupta et al., 2009; Green et al., 1992; Klemme and Meyer, 2003). HFSEs exhibit strong incompatibility characteristics during the crystallization process, and the fractionation of silicate and carbonate minerals increases the concentration of HFSEs in the residual melt (Adam and Green, 2001; Blundy and Dalton, 2000; Brenan and Watson, 1991; Dasgupta et al., 2009; Green et al., 1992; Klemme et al., 1995; Sweeney et al., 1995). Magmatic exsolution fluids can also remobilize HFSE and

transport them to form ore deposits (Salvi and Williams-Jones, 2006; Sheard et al., 2012). Overall, our research highlights the important role of Si partitioning and immiscibility in HFSE mineralization in carbonatite, and provides insights into the promising targets for future mineral exploration.

IMPLICATIONS

Our research provides new insights into the behavior of HFSEs during the formation of carbonatite melts via immiscibility with alkaline silicate magma. The partition coefficients of Nb, Ta, Zr, and Hf between carbonatite melt and silicate melt are positively correlated with the partition coefficient of Si, which increases with increasing temperature and decreasing pressure. Liquid immiscibility could lead to the depletion of HFSE and variation in Nb/Ta and Zr/Hf ratios in natural carbonatites. The presence of low SiO_2 levels in the silicate melt can lead to the efficient concentration of HFSEs in the carbonatite melt, reaching metallogenic grade. These findings suggest that carbonatitic melts containing higher HFSEs concentrations are more likely to occur during the early stages of the evolution process, which explains why super large carbonatite-related Nb deposits are associated with Si-undersaturated silicate rocks such as the melilitite and nephelinite. This research may have important implications for the exploration and development of HFSE deposits in carbonatites.

ACKNOWLEDGMENTS AND FUNDING

We thank Dr. Yonghua Cao for technical support and for ensuring that the electron probe analysis, and to Zhuoyu Liu for his support in high T–P experiments. We also extend our thanks to the two anonymous reviewers for their valuable comments in improving the quality of this article. This work is supported by the National Natural Science Foundation of China (No. 42173024), National Key R&D Program of China (2021YFC2901705), and Jiangxi Double Thousand Plan (DHSQT22021005).

REFERENCES CITED:

Adam, J., and Green, T. (2001) Experimentally determined partition coefficients for minor and trace elements in peridotite minerals and carbonatitic melt, and their relevance to natural carbonatites. European Journal of Mineralogy, 13(5), 815-827.

Anenburg, M., Broom-Fendley, S., and Chen, W. (2021) Formation of rare earth deposits in carbonatites. Elements, 17(5), 327-332.

Aral, H., and Bruckard, W. (2008) Characterisation of the Mt Weld (Western Australia) niobium ore. Mineral Processing Extractive Metallurgy, 117(4), 193-204.

Berndt, J., and Klemme, S. (2022) Origin of carbonatites—liquid immiscibility caught in the act. Nature communications, 13(1), 1-8.

Bizimis, M., Salters, V.J., and Dawson, J.B. (2003) The brevity of carbonatite sources in the mantle: evidence from Hf isotopes. Contributions to Mineralogy Petrology, 145(3), 281-300.

360 Blundy, J., and Dalton, J. (2000) Experimental comparison of trace element partitioning between
361 clinopyroxene and melt in carbonate and silicate systems, and implications for mantle
362 metasomatism. Contributions to Mineralogy Petrology, 139(3), 356-371.
363 Brenan, J.M., and Watson, E.B. (1991) Partitioning of trace elements between carbonate melt
364 and clinopyroxene and olivine at mantle PT conditions. Geochimica et Cosmochimica
365 Acta, 55(8), 2203-2214.
366 Brooker, R., and Kjarsgaard, B. (2011) Silicate–carbonate liquid immiscibility and phase relations
367 in the system SiO2–Na2O–Al2O3–CaO–CO2 at 0· 1–2· 5 GPa with applications to
368 carbonatite genesis. Journal of Petrology, 52(7-8), 1281-1305.
369 Castor, S. (2008) The Mountain Pass rare-earth carbonatite and associated ultrapotassic rocks,
370 California. Canadian Mineralogist - CAN MINERALOG, 46, 779-806.
371 Chakhmouradian, A.R. (2006) High-field-strength elements in carbonatitic rocks: geochemistry,
372 crystal chemistry and significance for constraining the sources of carbonatites. Chemical
373 Geology, 235(1-2), 138-160.
374 Dasgupta, R., and Hirschmann, M.M. (2006) Melting in the Earth's deep upper mantle caused by
375 carbon dioxide. Nature, 440(7084), 659-662.
376 Dasgupta, R., Hirschmann, M.M., McDonough, W.F., Spiegelman, M., and Withers, A.C. (2009)
377 Trace element partitioning between garnet lherzolite and carbonatite at 6.6 and 8.6 GPa
378 with applications to the geochemistry of the mantle and of mantle-derived melts.
379 Chemical Geology, 262(1-2), 57-77.

Dasgupta, R., Mallik, A., Tsuno, K., Withers, A.C., Hirth, G., and Hirschmann, M.M. (2013) Carbon-dioxide-rich silicate melt in the Earth's upper mantle. Nature, 493(7431), 211-215.

de Oliveira Cordeiro, P.F., Brod, J.A., Palmieri, M., de Oliveira, C.G., Barbosa, E.S.R., Santos, R.V., Gaspar, J.C., and Assis, L.C. (2011) The Catalão I niobium deposit, central Brazil: Resources, geology and pyrochlore chemistry. Ore Geology Reviews, 41(1), 112-121.

Fowler, A., Prokoph, A., Stern, R., and Dupuis, C. (2002) Organization of oscillatory zoning in zircon: analysis, scaling, geochemistry, and model of a zircon from Kipawa, Quebec, Canada. Geochimica et Cosmochimica Acta, 66(2), 311-328.

Freestone, I., and Hamilton, D. (1980) The role of liquid immiscibility in the genesis of carbonatites—an experimental study. Contributions to Mineralogy Petrology, 73(2), 105-117.

Green, T., Adam, J., and Siel, S. (1992) Trace element partitioning between silicate minerals and carbonatite at 25 kbar and application to mantle metasomatism. Mineralogy Petrology, 46(3), 179-184.

Hamilton, D., Bedson, P., and Esson, J. (1989) The behavior of trace element in the evolution of carbonatites. In: Bell, K., Ed., Carbonatites: Genesis and Evolution, Unwin Hyman, Boston, 405-427.

Hamilton, D., and Kjarsgaard, B. (1993) The immiscibility of silicate and carbonate liquids. South African journal of geology, 96(3), 139-142.

Hoernle, K., Tilton, G., Le Bas, M.J., Duggen, S., and Garbe-Schönberg, D. (2002) Geochemistry

of oceanic carbonatites compared with continental carbonatites: mantle recycling of oceanic crustal carbonate. Contributions to Mineralogy Petrology, 142(5), 520-542.

Hou, Z.Q., Liu, Y., Tian, S.H., Yang, Z.M., and Xie, Y.L. (2015) Formation of carbonatite-related giant rare-earth-element deposits by the recycling of marine sediments. Scientific Reports, 5(1), 10231.

Hou, Z.Q., Tian, S.H., Yuan, Z.X., Xie, Y.L., Yin, S.P., Sheng, Y.L., Fei, H.C., and Yang, Z.M. (2006) The Himalayan collision zone carbonatites in western Sichuan, SW China: Petrogenesis, mantle source and tectonic implication. Earth and Planetary Science Letters, 244, 234-250.

Humphreys-Williams, E.R., and Zahirovic, S. (2021) Carbonatites and global tectonics. Elements: An International Magazine of Mineralogy, Geochemistry, Petrology, 17(5), 339-344.

Ivanyuk, G.Y., Kalashnikov, A., Pakhomovsky, Y.A., Mikhailova, J., Yakovenchuk, V., Konopleva, N., Sokharev, V., Bazai, A., and Goryainov, P. (2016) Economic minerals of the Kovdor baddeleyite-apatite-magnetite deposit, Russia: Mineralogy, spatial distribution and ore processing optimization. Ore Geology Reviews, 77, 279-311.

Kjarsgaard, B., and Hamilton, D. (1989) Carbonatite origin and diversity. Nature, 338(6216), 547-548.

Klemme, S., and Meyer, H.-P. (2003) Trace element partitioning between baddeleyite and carbonatite melt at high pressures and high temperatures. Chemical Geology, 199(3-4), 233-242.

Klemme, S.v., Van der Laan, S., Foley, S.F., and Günther, D. (1995) Experimentally determined trace and minor element partitioning between clinopyroxene and carbonatite melt under upper mantle conditions. Earth Planetary Science Letters, 133(3-4), 439-448.

Lazareva, E., Zhmodik, S., Dobretsov, N., Tolstov, A., Shcherbov, B., Karmanov, N., Gerasimov, E.Y., and Bryanskaya, A. (2015) Main minerals of abnormally high-grade ores of the Tomtor deposit (Arctic Siberia). Russian geology geophysics, 56(6), 844-873.

Lee, W.-j., and Wyllie, P.J. (1994) Experimental data bearing on liquid immiscibility, crystal fractionation, and the origin of calciocarbonatites and natrocarbonatites. International Geology Review, 36(9), 797-819.

-. (1997) Liquid immiscibility between nephelinite and carbonatite from 1.0 to 2.5 GPa compared with mantle melt compositions. Contributions to Mineralogy Petrology, 127(1), 1-16.

Ling, M.-X., Liu, Y.L., Williams, I.S., Teng, F.Z., Yang, X.Y., Ding, X., Wei, G.J., Xie, L.H., Deng, W.F., and Sun, W.D. (2013) Formation of the world's largest REE deposit through protracted fluxing of carbonatite by subduction-derived fluids. Scientific reports, 3(1), 1-8.

Liu, Y., Chakhmouradian, A.R., Hou, Z., Song, W., and Kynický, J. (2019) Development of REE mineralization in the giant Maoniuping deposit (Sichuan, China): insights from mineralogy, fluid inclusions, and trace-element geochemistry. Mineralium Deposita, 54(5), 701-718.

Mackay, D.A., and Simandl, G.J. (2014) Geology, market and supply chain of niobium and tantalum—a review. Mineralium Deposita, 49, 1025-1047.

Martin, L.H., Schmidt, M.W., Mattsson, H.B., and Guenther, D. (2013) Element partitioning

between immiscible carbonatite and silicate melts for dry and H2O-bearing systems at 1–3 GPa. Journal of Petrology, 54(11), 2301-2338.

Martin, L.H., Schmidt, M.W., Mattsson, H.B., Ulmer, P., Hametner, K., and Günther, D. (2012) Element partitioning between immiscible carbonatite–kamafugite melts with application to the Italian ultrapotassic suite. Chemical Geology, 320, 96-112.

Mitchell, R.H. (2005) Carbonatites and carbonatites and carbonatites. The Canadian Mineralogist, 43(6), 2049-2068.

Mitchell, R.H. (2015) Primary and secondary niobium mineral deposits associated with carbonatites. Ore Geology Reviews, 64, 626-641.

Nabyl, Z., Gaillard, F., Tuduri, J., and Di Carlo, I.J.C.R.G. (2021) No direct effect of F, Cl and P on REE partitioning between carbonate and alkaline silicate melts. Comptes Rendus. Géoscience, 353(S2), 233-272.

Nabyl, Z., Massuyeau, M., Gaillard, F., Tuduri, J., Iacono-Marziano, G., Rogerie, G., Le Trong, E., Di Carlo, I., Melleton, J., and Bailly, L.J.G.e.C.A. (2020) A window in the course of alkaline magma differentiation conducive to immiscible REE-rich carbonatites. Geochimica et Cosmochimica Acta, 282, 297-323.

Palmieri, M., Brod, J.A., Cordeiro, P., Gaspar, J.C., Barbosa, P.A.R., de Assis, L.C., Junqueira-Brod, T.C., Silva, S.E.e., Milanezi, B.P., Machado, S.A., and Jácomo, M.H. (2022) The Carbonatite-Related Morro do Padre Niobium Deposit, Catalão II Complex, Central Brazil. Economic Geology, 117(7), 1497-1520.

460 Pfänder, J.A., Münker, C., Stracke, A., and Mezger, K. (2007) Nb/Ta and Zr/Hf in ocean island
461 basalts—implications for crust–mantle differentiation and the fate of Niobium. Earth
462 Planetary Science Letters, 254(1-2), 158-172.
463 Poletti, J.E., Cottle, J.M., Hagen-Peter, G.A., and Lackey, J.S. (2016) Petrochronological
464 Constraints on the Origin of the Mountain Pass Ultrapotassic and Carbonatite Intrusive
465 Suite, California. Journal of Petrology, 57(8), 1555-1598.
466 Rudnick, R.L., McDonough, W.F., and Chappell, B.W. (1993) Carbonatite metasomatism in the
467 northern Tanzanian mantle: petrographic and geochemical characteristics. Earth
468 Planetary Science Letters, 114(4), 463-475.
469 Salvi, S., and Williams-Jones, A.E. (2006) Alteration, HFSE mineralisation and hydrocarbon
470 formation in peralkaline igneous systems: Insights from the Strange Lake Pluton, Canada.
471 Lithos, 91(1-4), 19-34.
472 Sheard, E.R., Williams-Jones, A.E., Heiligmann, M., Pederson, C., and Trueman, D.L. (2012)
473 Controls on the concentration of zirconium, niobium, and the rare earth elements in the
474 Thor Lake rare metal deposit, Northwest Territories, Canada. Economic Geology, 107(1),
475 81-104.
476 Su, J.H., Zhao, X.F., Li, X.C., Hu, W., Chen, M., and Xiong, Y.L. (2019) Geological and
477 Geochemical Characteristics of the Miaoya Syenite-Carbonatite Complex , Central
478 China:Implications for the Origin of REE-Nb-enriched Carbonatite. Ore Geology Reviews,
479 113, 103101.

480 Sweeney, R., Prozesky, V., and Przybylowicz, W. (1995) Selected trace and minor element
481 partitioning between peridotite minerals and carbonatite melts at 18–46 kb pressure.
482 Geochimica et Cosmochimica Acta, 59(18), 3671-3683.
483 Tang, M., Lee, C.-T.A., Chen, K., Erdman, M., Costin, G., and Jiang, H. (2019) Nb/Ta systematics
484 in arc magma differentiation and the role of arclogites in continent formation. Nature
485 Communications, 10(1), 1-8.
486 Tappe, S., Romer, R.L., Stracke, A., Steenfelt, A., Smart, K.A., Muehlenbachs, K., and Torsvik,
487 T.H. (2017) Sources and mobility of carbonate melts beneath cratons, with implications
488 for deep carbon cycling, metasomatism and rift initiation. Earth Planetary Science Letters,
489 466, 152-167.
490 Veksler, I., Petibon, C., Jenner, G., Dorfman, A., and Dingwell, D. (1998) Trace element
491 partitioning in immiscible silicate–carbonate liquid systems: an initial experimental study
492 using a centrifuge autoclave. Journal of Petrology, 39(11-12), 2095-2104.
493 Veksler, I.V., Dorfman, A.M., Dulski, P., Kamenetsky, V.S., Danyushevsky, L.V., Jeffries, T., and
494 Dingwell, D.B. (2012) Partitioning of elements between silicate melt and immiscible
495 fluoride, chloride, carbonate, phosphate and sulfate melts, with implications to the origin
496 of natrocarbonatite. Geochimica et Cosmochimica Acta, 79, 20-40.
497 Verplanck, P.L., Mariano, A.N., Mariano, A., Jr., Verplanck, P.L., and Hitzman, M.W. (2016) Rare
498 Earth Element Ore Geology of Carbonatites. Rare Earth and Critical Elements in Ore
499 Deposits, 18, p. 0. Society of Economic Geologists.

500 Wallace, M.E., and Green, D.H. (1988) An experimental determination of primary carbonatite
501 magma composition. Nature, 335(6188), 343-346.
502 Wang, C., Liu, J.C., Zhang, H.D., Zhang, H.D., Zhang, X.Z., Zhang, D.M., Xi, Z.X., and Wang, Z.J.
503 (2019) Geochronology and mineralogy of the Weishan carbonatite in Shandong province,
504 eastern China. Geoscience Frontiers, 10(2), 769-785.
505 Wang, D.H., Yang, J.M., Yan, S.H., Xu, J., Chen, Y.C., Pu, G.P., and Luo, Y.N. (2001) A Special
506 Orogenic-type Rare Earth Element Deposit in Maoniuping, Sichuan, China: Geology and
507 Geochemistry. Resource Geology, 51, 177-188.
508 Weidendorfer, D., and Asimow, P.D. (2022) Experimental constraints on truly conjugate alkaline
509 silicate–carbonatite melt pairs. Earth Planetary Science Letters, 584, 117500.
510 Woolley, A.R., and Kjarsgaard, B.A. (2008) Carbonatite occurrences of the world. Geological
511 Survey of Canada, Geological Survey of Canada.
512 Xu, C., Huang, Z.L., Liu, C.Q., Qi, L., Li, W.B., and Guan, T. (2003) Geochemistry of carbonatites
513 in Maoniuping REE deposit, Sichuan province, China. Science in China Series D: Earth
514 Sciences, 46(3), 246-256.
515 Xue, S., Ling, M.-X., Liu, Y.L., Kang, Q.Q., Huang, R.F., Zhang, Z.K., and Sun, W.d. (2020) The
516 formation of the giant Huayangchuan U-Nb deposit associated with carbonatite in the
517 Qingling Orogenic Belt. Ore Geology Reviews, 122, 103498.
518 Yang, K., Fan, H., Pirajno, F., and Li, X. (2019) The Bayan Obo (China) giant REE accumulation
519 conundrum elucidated by intense magmatic differentiation of carbonatite. Geology,

47(12), 1198-1202.

Yang, K.F., Fan, H.R., Pirajno, F., and Liu, X. (2023) Magnesium isotope fractionation in differentiation of mafic-alkaline-carbonatitic magma and Fe-P-REE-rich melt at Bayan Obo, China. Ore Geology Reviews, 157, 105466.

Yaxley, G.M., Anenburg, M., Tappe, S., Decree, S., and Guzmics, T. (2022) Carbonatites: classification, sources, evolution, and emplacement. Annual Review of Earth Planetary Sciences, 50, 261-293.

Zhang, D.X., Liu, Y., Pan, J.Q., Dai, T., and Bayless, R. (2019) Mineralogical and Geochemical Characteristics of the Miaoya REE Prospect, Qinling Orogenic Belt, China: Insights from Sr-Nd-C-O Isotopes and LA-ICP-MS Mineral Chemistry. Ore Geology Reviews, 110.

Figure captions

Figure 1. Backscattered Electron (BSE) images depicting immiscible silicate and carbonatitic liquids. Panels (a) and (b) exhibit the characteristic two-liquid textures, where spherical silicate liquids (SL) are enclosed by rapidly quenched carbonatitic melt (CM) from experiments 2.2-1200-0 and 1.5-1200-4%S, respectively. For a closer examination, panels (c) and (d) provide detailed views of runs 2.2-1200-4%S and 1.5-1100-4%S. In these images, silicate melts are represented as homogeneous spherical glasses, while carbonatitic melts manifest as dendritic crystals composed of carbonates and silicates. Panels (e) and (f) display the typical carbonatitic and silicate liquid

immiscibility from runs 1.5-1200-1%F and 1.5-1150-4%S.

Figure 2. Correlation diagrams show the HFSEs (y-axis) and Si (x-axis) partition coefficients from both this study and previous investigations. (a) Si and Nb partition coefficients, (b) Si and Ta partition coefficients, (c) Si and Zr partition coefficients, and (d) Si and Hf partition coefficients, (e) Si and Nb/Ta and (f) Si and Zr/Hf. Grey symbols in the figure were collected from previous studies (Martin et al., 2013; Martin et al., 2012; Nabyl et al., 2021; Nabyl et al., 2020; Veksler et al., 2012). Notably, the scatter plot highlights a clear positive correlation between Si partition coefficient and HFSEs partition coefficient. Furthermore, negative correlations between Si partition coefficient and Nb/Ta and Zr/Hf partition coefficient ratios are observed.

Figure 3. (a) The effect of immiscibility to modify HFSE concentrations in carbonatitic melt. (b) The effect of immiscibility to modify Nb/Ta and Zr/Hf ratios in carbonatitic melt. The fractionated carbonatitic melt is represented by CM and the initial carbonated silicate melt by IM. Detailed simulation procedures are shown in the main text.

Figure 4. Schematic diagram shows the controlling effect of different liquid immiscibility processes on the mineralization of HFSE. (a) Under shallow crustal and

high-temperature conditions, the differentiated carbonatite melt is more enriched in HFSE, which is favorable for mineralization. (b) Under deep crustal and low-temperature conditions, the differentiated carbonatite melt is deficient in HFSE, which is unfavorable for mineralization. The picture is adapted from (Yang et al., 2019).

Table 1. Major and trace element compositions of the starting material.

Major element（wt.%）	
SiO_2	16.48
Al_2O_3	4.67
Na_2CO_3	4.87
$CaCO_3$	42.99
Na_2CO_3	31
Total	100
Trace elements in ppm	
Ta	100
Hf	100
Zr	100
Nb	100

Table 2. Summary of the experimental conditions and run products.

Exp. ID	Starting materials*	Temperature (°C)	Pressure (GPa)	Capsule	Run duration (Hours)	Run products
1.5-1200-0	RB100	1200	1.5	Pt	30	CM+ SL
1.5-1200-1S	99% RB100 + 1% $CaSO_4$	1200	1.5	Pt	30	CM+ SL
1.5-1200-2S	98% RB100 + 2% $CaSO_4$	1200	1.5	Pt	30	CM+ SL
1.5-1200-4S	96% RB100 + 4% $CaSO_4$	1200	1.5	Pt	30	CM+ SL
1.5-1200-1F	99% RB100 + 1% MgF_2	1200	1.5	Pt	30	CM+ SL
1.5-1200-2F	98% RB100 + 2% MgF_2	1200	1.5	Pt	30	CM+ SL
1.5-1200-4F	96% RB100 + 4% MgF_2	1200	1.5	Pt	30	CM+ SL
0.5-1200-0	RB100	1200	0.5	Pt	30	CM+ SL
0.5-1200-4S	96% RB100 + 4% $CaSO_4$	1200	0.5	Pt	30	CM+ SL
2.2-1200-0	RB100	1200	2.2	Pt	30	CM+ SL
2.2-1200-4S	96% RB100 + 4% $CaSO_4$	1200	2.2	Pt	30	CM+ SL
1.5-1150-0	RB100	1150	1.5	Pt	48	CM+ SL
1.5-1150-4S	96% RB100 + 4% $CaSO_4$	1150	1.5	Pt	48	CM+ SL
1.5-1150-4F	96% RB100 + 4% MgF_2	1150	1.5	Pt	48	CM+ SL
1.5-1100-0	RB100	1100	1.5	Pt	48	CM+ SL
1.5-1100-4S	96% RB100 + 4% $CaSO_4$	1100	1.5	Pt	48	CM+ SL
1.5-1100-4F	96% RB100 + 4% MgF_2	1100	1.5	Pt	48	CM+ SL
1.5-1000-0	RB100	1000	1.5	Pt	72	CM+ SL
1.5-1000-4S	96% RB100 + 4% $CaSO_4$	1000	1.5	Pt	72	CM+ SL

CM=Quenched carbonatitic melt; SL=silicate liqui

*The starting material used for the experiments consisted of a mixture composition (#RB100) from Brooker and Kjarsgaard (2011).

Table 3. Calculated partition coefficients for major and trace elements between carbonatitic melt and silicate melt.

KD	SiO_2	SO_3	F	Zr	Nb	Hf	Ta
1.5-1200-0	0.17			0.2	0.76	0.14	0.35
σ	0.05			0.02	0.08	0.01	0.03
1.5-1200-1S	0.22	1.79		0.2	0.68	0.15	0.37
σ	0.03	0.39		0.02	0.02	0.01	0.01
1.5-1200-2S	0.31	1.62		0.37	0.8	0.3	0.52
σ	0.09	0.31		0.13	0.21	0.11	0.15
1.5-1200-4S	0.24	3.23		0.24	0.75	0.2	0.4
σ	0.06	0.66		0.04	0.08	0.03	0.05
1.5-1200-1F	0.15		7.12	0.23	0.71	0.16	0.34
σ	0.05		2.86	0.03	0.05	0.02	0.03
1.5-1200-2F	0.2		4.93	0.2	0.66	0.15	0.33
σ	0.06		1.38	0.05	0.06	0.04	0.05
1.5-1200-4F	0.44		3.35	0.27	0.5	0.23	0.34
σ	0.05		0.33	0.06	0.04	0.06	0.05
0.5-1200-0	0.61			0.45	0.73	0.43	0.61
σ	0.03			0.02	0.05	0.01	0.02
0.5-1200-4S	0.25	4.34		0.16	0.64	0.13	0.4
σ	0.02	0.97		0.03	0.02	0.02	0.03
2.2-1200-0	0.04			0.17	0.44	0.06	0.12
σ	0.03			0.11	0.07	0.01	0.03
2.2-1200-4S	0.08	9.54		0.21	0.61	0.13	0.23
σ	0.06	3.95		0.04	0.07	0.02	0.03
1.5-1150-0	0.07			0.08	0.51	0.04	0.18
σ	0.01			0.01	0.04	0	0.01
1.5-1150-4S	0.16	9.25		0.16	0.64	0.11	0.29
σ	0.06	1.93		0.04	0.1	0.03	0.05
1.5-1150-4F	0.09		4.55	0.21	0.52	0.19	0.26
σ	0.04		0.44	0.08	0.11	0.08	0.09
1.5-1100-0	0.07			0.1	0.44	0.05	0.14
σ	0.04			0.04	0.06	0.01	0.02
1.5-1100-4S	0.07	8.48		0.19	0.83	0.12	0.3
σ	0.03	2.45		0.02	0.05	0.02	0.01
1.5-1100-4F	0.19		4.97	0.19	0.62	0.14	0.27
σ	0.07		1.41	0.07	0.12	0.05	0.08
1.5-1000-0	0.04			0.09	0.5	0.04	0.13
σ	0.04			0.02	0.05	0.01	0.02
1.5-1000-4S	0.06	10.8		0.06	0.48	0.03	0.1
σ	0.01	3.15		0.01	0.03	0	0.01

Table 4. Calculated coefficients and associated errors used for the modelling.

	a (1/T)	σ	b (P/T)	σ	c	σ	d ($logD_{Si}$)	σ	R^2
Nb			95.6	47.7	-0.04	0.04	0.31	0.04	0.84
Ta	-1805	800			1.09	0.52	0.46	0.08	0.82
Zr	-2895	1031			1.54	0.68	0.3	0.11	0.7
Hf	-2433	1290			1.3	0.85	0.6	0.13	0.76
Nb/Ta	1580	390	93.9	53.7	-1.08	0.26	-0.27	0.05	0.93
Zr/Hf					-0.06	0.04	-0.27	0.04	0.7

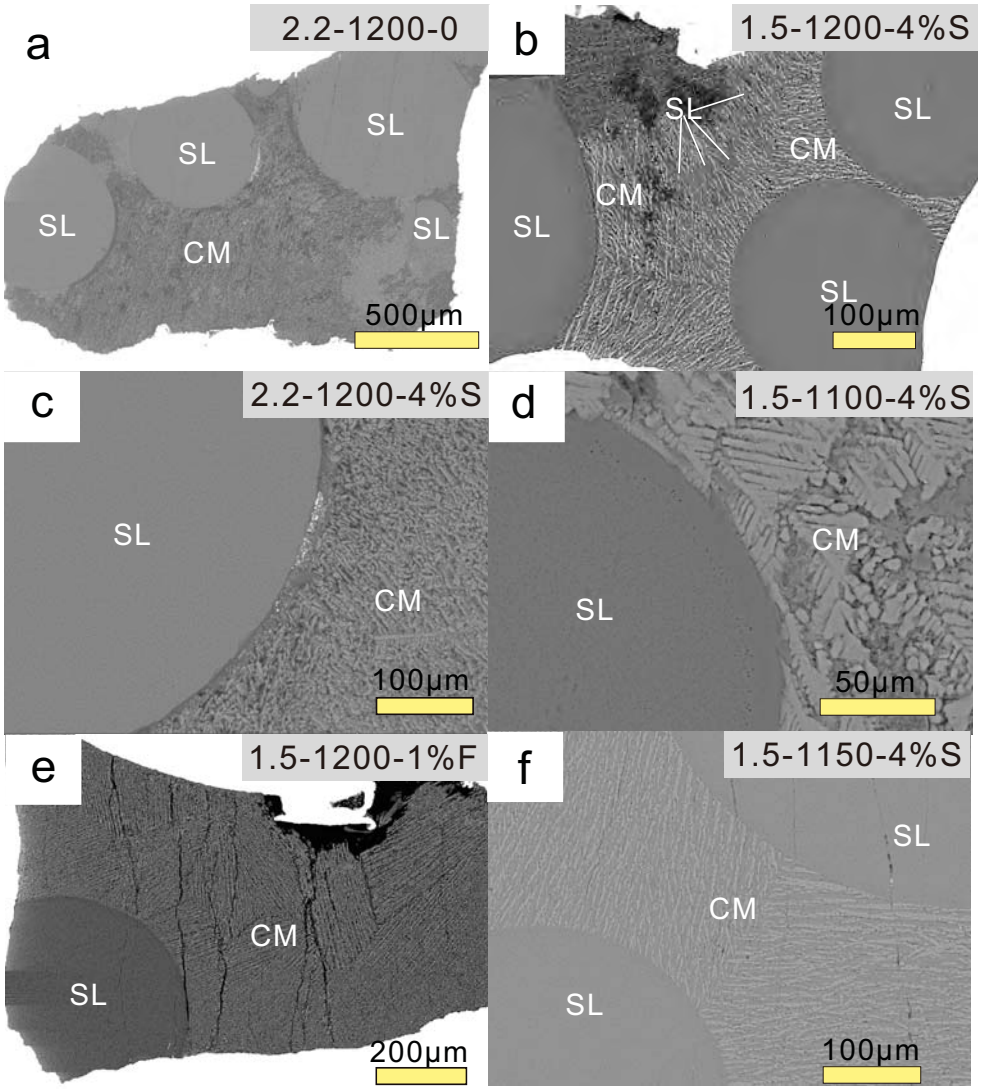
a
2.2-1200-0
SL
SL
SL
SL
CM
SL
500μm
b
1.5-1200-4%S
SL
SL
CM
CM
SL
SL
100μm
c
2.2-1200-4%S
SL
CM
100μm
d
1.5-1100-4%S
CM
SL
50μm
e
1.5-1200-1%F
CM
SL
200μm
f
1.5-1150-4%S
SL
CM
SL
100μm

Fig. 1

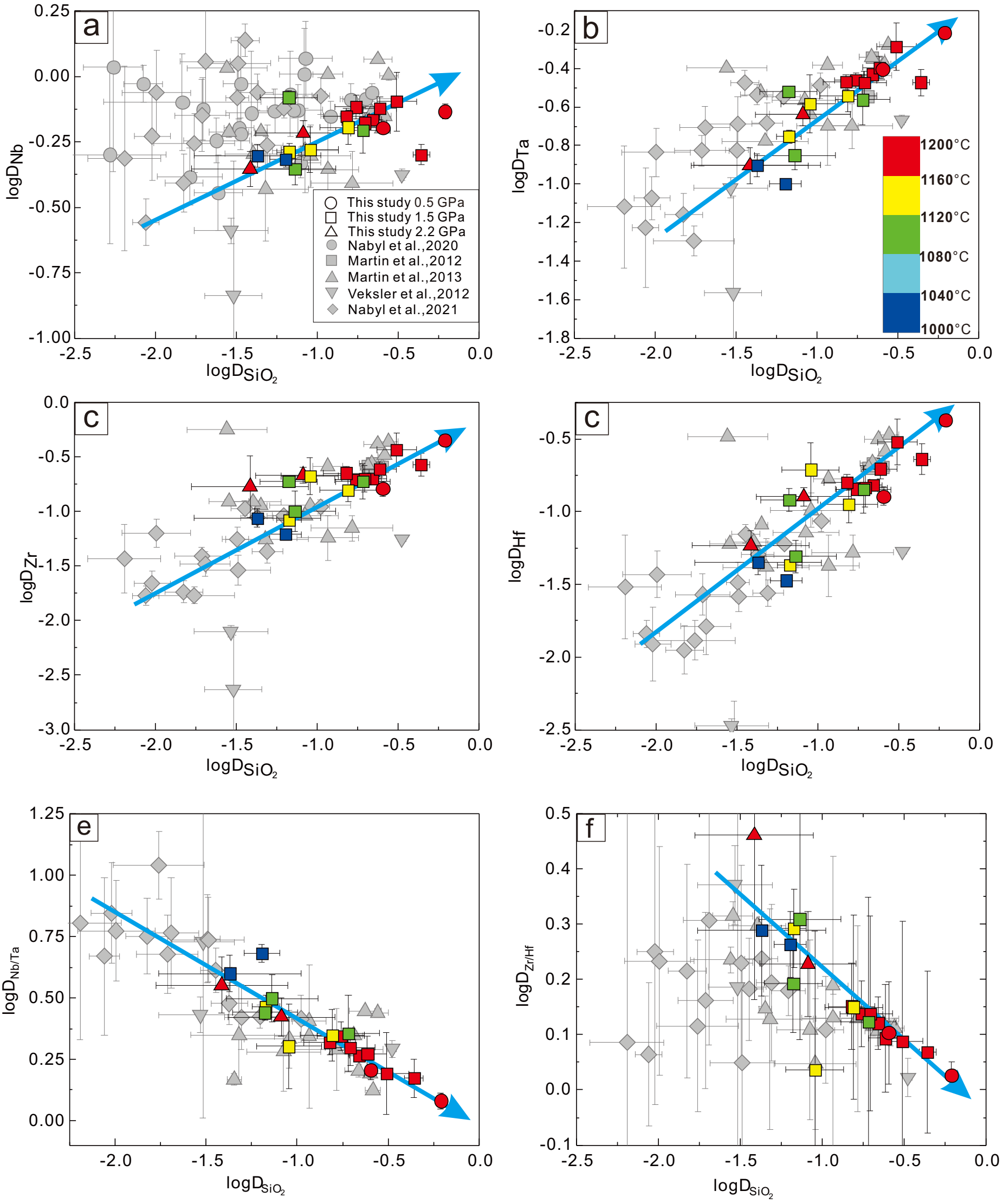
a
b
c
c
e
f
logDNb
logDTa
logDZr
logDHf
logDNb/Ta
logDZr/Hf
logDSiO2
This study 0.5 GPa
This study 1.5 GPa
This study 2.2 GPa
Nabyl et al.,2020
Martin et al.,2012
Martin et al.,2013
Veksler et al.,2012
Nabyl et al.,2021
1200°C
1160°C
1120°C
1080°C
1040°C
1000°C

Fig. 2

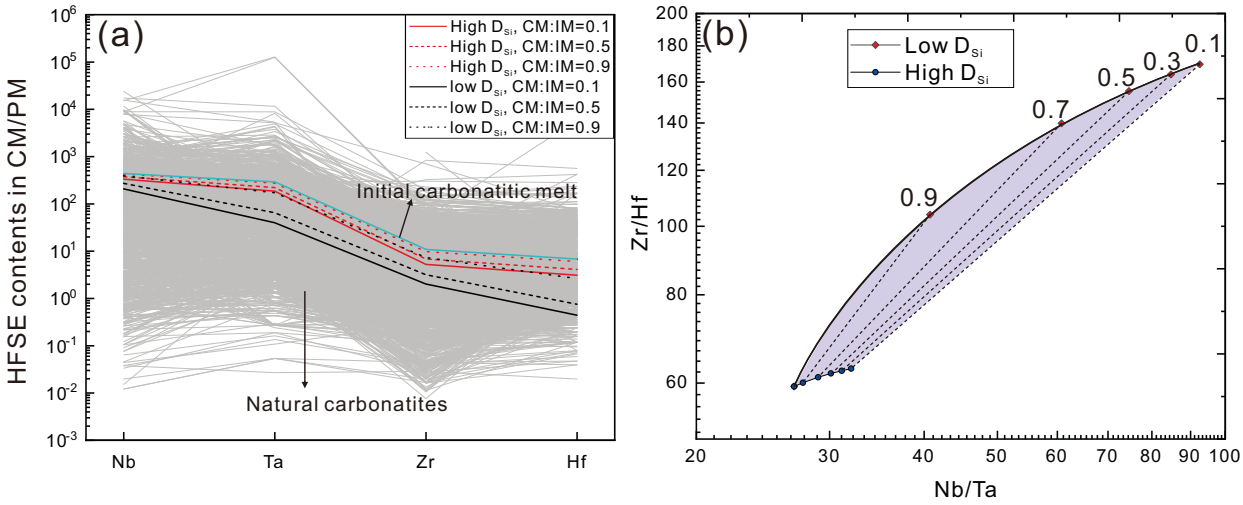
(a)
High D_{Si}, CM:IM=0.1
High D_{Si}, CM:IM=0.5
High D_{Si}, CM:IM=0.9
low D_{Si}, CM:IM=0.1
low D_{Si}, CM:IM=0.5
low D_{Si}, CM:IM=0.9
Initial carbonatitic melt
Natural carbonatites
HFSE contents in CM/PM
Nb
Ta
Zr
Hf
(b)
Low D_{Si}
High D_{Si}
0.9
0.7
0.5
0.3
0.1
Zr/Hf
Nb/Ta

Fig. 3

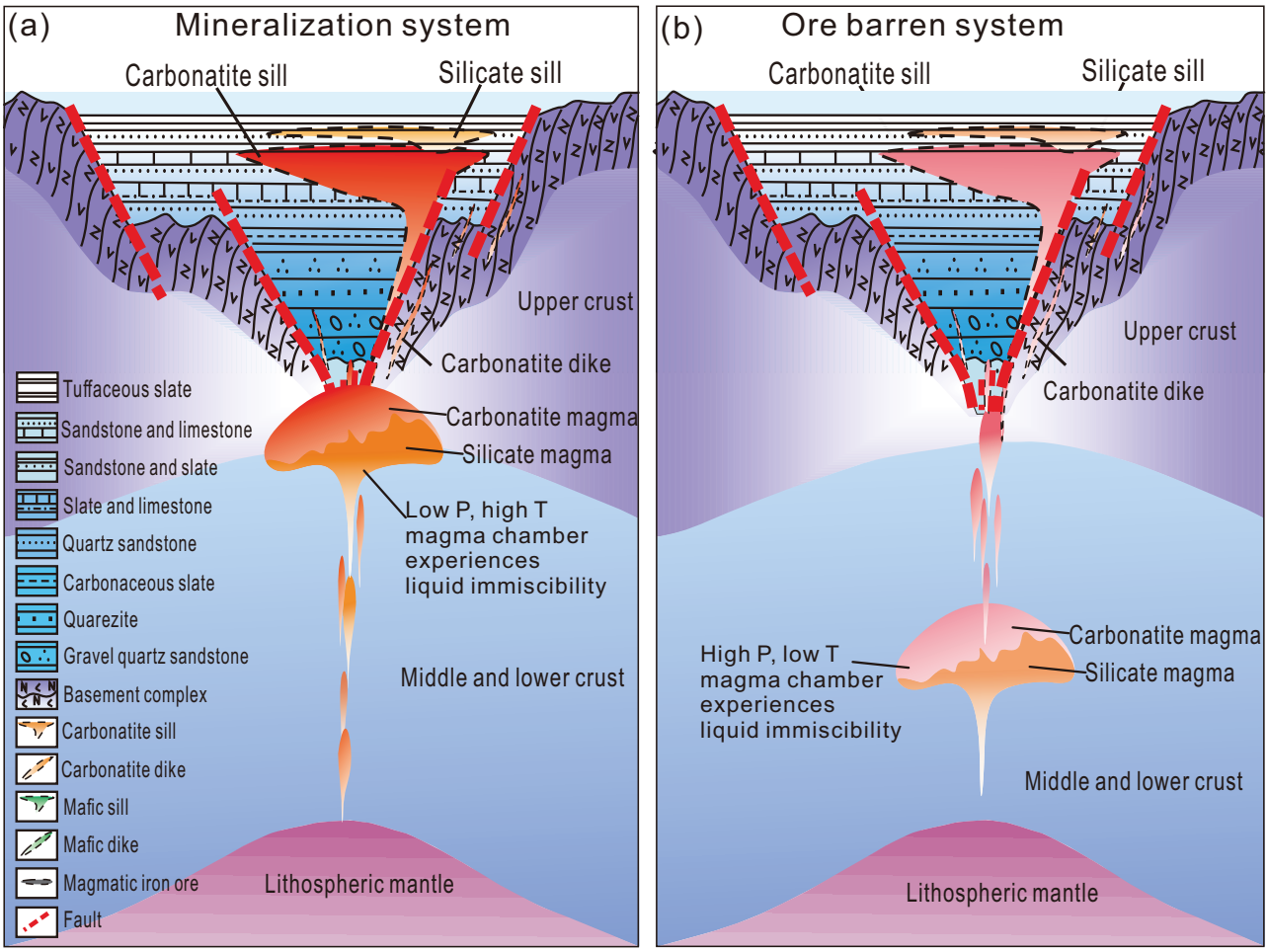
(a)
Mineralization system
Carbonatite sill
Silicate sill
Upper crust
Carbonatite dike
Carbonatite magma
Silicate magma
Low P, high T
magma chamber
experiences
liquid immiscibility
Middle and lower crust
Lithospheric mantle
Tuffaceous slate
Sandstone and limestone
Sandstone and slate
Slate and limestone
Quartz sandstone
Carbonaceous slate
Quarezite
Gravel quartz sandstone
Basement complex
Carbonatite sill
Carbonatite dike
Mafic sill
Mafic dike
Magmatic iron ore
Fault
(b)
Ore barren system
Carbonatite sill
Silicate sill
Upper crust
Carbonatite dike
Carbonatite magma
Silicate magma
High P, low T
magma chamber
experiences
liquid immiscibility
Middle and lower crust
Lithospheric mantle

Fig. 4